Differential intensity contrast swept source optical coherence tomography for human retinal vasculature visualization

Reza Motaghiannezam and Scott Fraser

Beckman Institute, Division of Biology, California Institute of Technology, Pasadena, California 91125-7400

ABSTRACT

We demonstrate an intensity-based motion sensitive method, called differential logarithmic intensity variance (DLOGIV), for 3D microvasculature imaging and foveal avascular zone (FAZ) visualization in the *in vivo* human retina using swept source optical coherence tomography (SS-OCT) at 1060 nm. A motion sensitive SS-OCT system was developed operating at 50,000 A-lines/s with 5.9 μm axial resolution, and used to collect 3D images over 4 mm^2 in a normal subject eye. Multiple B-scans were acquired at each individual slice through the retina and the variance of differences of logarithmic intensities as well as the differential phase variances (DPV) was calculated to identify regions of motion (microvasculature). En face DLOGIV image were capable of capturing the microvasculature through depth with an equal performance compared to the DPV.

Keywords: Optical coherence tomography, Fourier Domain, Coherence imaging, Medical and biological imaging, Optical Coherence Angiography, Ophthalmology

1. INTRODUCTION

Recent studies suggest the importance of imaging the retinal and choroidal vasculature networks in diagnosing various eye diseases, such as diabetic retinopathy[1], age-related macular degeneration (AMD)[2], glaucoma[3], and anterior ischemic optic neuropathy (AION)[4].

Color fundus photography (CF) and fluorescein angiography (FA) have served as valuable imaging methods for retinal vasculature network visualization[5]. Deeper choroidal vessel imaging has also been realized by Indocyanine green angiography (ICGA)[5]. However, fluorescent dye injection can cause undesired side-effects[6,7], and the 2-D nature of these imaging techniques limits their applications for providing depth information and/or deep choroidal blood vessel visualization.

To meet the need for 3D retinal and choroidal vasculature assessment without the use of fluorescent dye injection, optical coherence tomography (OCT) has emerged as an attractive non-invasive depth-resolved imaging technology[8]. OCT realizes 3D visualization of retinal structure[9] and vasculature[10] by capturing interferograms of the light reflected back from the retina. Doppler OCT (D-OCT)[11] and Phase Contrast (PC)-OCT[12] are motion sensitive methods for vessel visualization, since these methods collect more than one depth scan of the same retinal loci and analyze Doppler phase shifts between depth scans at different depths. Although D-OCT captures the regions of high-velocity blood flow, such as in major vessels, it is unable to capture slow flow in retinal capillaries[11] or deep flows such as the choroidal circulation due to limited phase sensitivity and small time separation between two successive A-scans. Smart scanning protocols enhance sensitivity to the smaller signals expected from the microvasculature by increasing the time separation between two OCT depth scans and relying on the acquired phase[12-15] of OCT signals for contrast. However, these methods[13-15] such as PC-OCT[12] are highly sensitive to the phase instability of the system and environment by relying on the phase information. The required bulk motion removal[16] and timing-induced phase error correction algorithms[17] as well as extra optical module[17] add to the complexity of the phase sensitive swept source (SS)-OCT software and hardware.

To avoid complications of the phase instability in retinal microvasculature visualization, several elegant intensity contrast imaging methods have relied on the temporal speckle fluctuations caused by mobile particles, such as red blood cells. The first method captured microvasculature through Hilbert and Fourier analyses of the spectral domain (SD)-OCT signal and a moving reference arm[18,19]. However, the system complexity and high sensitivity to hyper-reflective static layers may limit its clinical application for distinguishing these areas from regions of motion. Another approach used speckle signals[20,21], which have been studied extensively in the literature[22-25]. Although this speckle variance imaging method was able to capture vessels no smaller than 25 μm diameter size in the mouse dorsal skinfold[20,21], the

Ophthalmic Technologies XXII, edited by Fabrice Manns, Per G. Söderberg, Arthur Ho,
Proc. of SPIE Vol. 8209, 82090O · © 2012 SPIE · CCC code: 1605-7422/12/$18 · doi: 10.1117/12.907149

multiplicative nature of the speckle made its variance highly sensitive to static regions similar to the first method[18,19], as shown in our results.

Thus, there is a need for a simple OCT method which does not rely on the phase information and provides highly motion-sensitive contrast for distinguishing regions of motion from stationary areas. The latter is especially important for detecting leakage and abnormal vessels in patients with abnormal retinal and choroidal structure.

Here, we purpose a motion-sensitive logarithmic intensity-based contrast for 3D microvasculature visualization in an *in vivo* human retina. The proposed logarithm operation converts the multiplicative amplitude fluctuations (speckle) into the additive variations and recovers the motion contrast by removing the speckle free signals (static regions) through statistical analysis. We develop a method, called differential logarithmic intensity variance (DLOGIV), which provides a surrogate marker for motion by acquiring more than one depth scan of the same retinal voxel and analyzing logarithmic intensity fluctuations at the same voxel. Application of DLOGIV for 3D microvasculature imaging in the *in vivo* human retina is validated by employing a high-speed SS-OCT at 1060 nm. Compared to the differential phase contrast method[12], this logarithmic intensity-based motion contrast method is simpler, has similar performance, and does not require extra software and hardware[17].

2. METHODS

2.1 SS-OCT system

To validate the proposed intensity-based method for providing motion contrast and compare it with DPV method[12,15], we used a prototype 50 kHz phase sensitive SS-OCT system, incorporating a polygon-based 1060 nm (1015-1103) swept laser source[26], with ~5.9 μm axial resolution in tissue and 102 dB sensitivity (1.2 mW incident power). The SS-OCT system was comprised of the polygon-based swept-laser source[26], an interferometer, and a data acquisition (DAQ) unit (Fig. 1). The swept source output was coupled to the interferometer through an isolator where a 90/10 coupler was used to split light into a sample arm : reference arm. The sample arm light was split equally between the calibration arm and a slit lamp biomicroscope (Carl Zeiss Meditec) as shown in Fig. 1. A 50/50 coupler combined and directed the reflected light from the sample to the one port of the interferometer output coupler. The reference arm light passed through a pair of collimators and was directed to the second port of the interferometer output coupler. The resulting interference fringes were detected on both output ports using a dual balanced photodetector. To generate a trigger signal at the beginning of the first interference fringe for data acquisition, a portion of the reference arm light was directed to a three port circulator and a fiber Bragg grating. A reflected optical pulse was detected using a photodetector and converted into an electronically tunable TTL signal as a trigger signal. The spectral signals were continuously digitized by triggering an AD conversion board. A D/A board was used to generate the driving signals of the two-axis galvanometers. A user interface and data acquisition was developed in LabView to coordinate instrument control and enable user interaction.

2.2 Scanning protocols

The prototype SS-OCT instrument was used to image the eye of a healthy volunteer (37-year-old Caucasian male) at the California Institute of Technology (Caltech). This study was approved by the Caltech committee for the protection of human subjects and adhered to the tenets of the Declaration of Helsinki. Written informed consent was obtained from subjects prior to OCT imaging. Total exposure time and incident exposure level were kept less than 5.5 seconds and 1.2 mW in each imaging session, consistent with the safe exposure determined by American National Standards Institute (ANSI) and International Commission on Non-Ionizing Radiation Protection (ICNIRP). Patient interfaces were based on a Stratus OCT-3 system (Carl Zeiss Meditec) adapted with optics to support the 1060 nm wavelength range. A 60-D lens was used at the exit of the fundus camera with 13 mm working distance providing a beam diameter of 1.5 mm on the cornea (~15 μm transverse resolution).

Two scanning protocols were implemented. A 2D protocol acquired four horizontal tomograms (B-scans) with 201 depth scans (A-scans) spanning the same transverse slice (2 mm) across the foveal centralis in 0.02 seconds. In the second protocol, a 3D OCT data set was collected by acquiring several neighboring B-scans over the parafovea. The system magnification, SS-OCT speed (50400 Hz), speed of the fast scan axis (200 Hz) with fly-back time (1 ms) , and data acquisition time (4 seconds) gave an image size of 201 × 200 pixels over a 2 mm × 2 mm field of view (FOV); each B-scan was repeated four times. In the 3D scanning protocol, the fast scan axis was sagittal (superior-inferior) and the slow axis was horizontal (nasal-temporal).

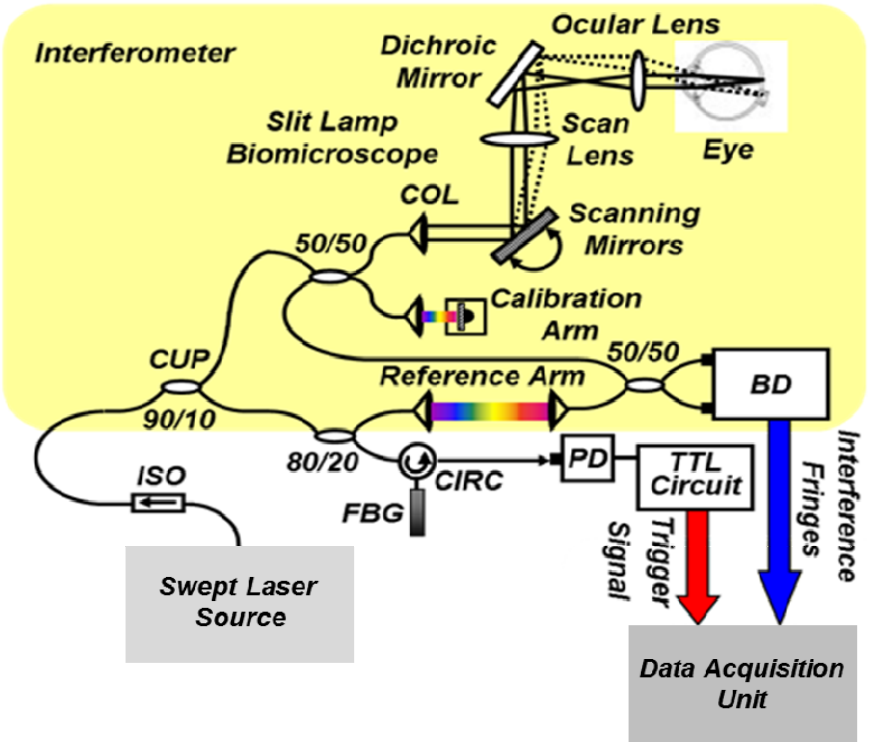

Fig. 1. Schematic of a polygon-based swept-laser source (gray box), interferometer (yellow box), and SS-OCT data acquisition unit (dark gray box) used for imaging. COL, collimator; PC, polarization controller; ISO, isolator; CIRC, circulator; CUP, coupler; PD, photodetector; BD, dual balanced photodetector (InGaAs, 80 MHz); FBG, fiber Bragg grating (0.1 nm). Data acquisition unit comprising of an AD conversion board (14-bit, GaGe CompuScope 14,200) for digitizing interference fringes and a D/A board (16 bit, National Instruments) for driving scanning mirrors (Cambridge Technology).

2.3 Image processing and motion contrast imaging

The digitized signals were divided into individual spectral sweeps in the post-processing algorithm. Equal sample spacing in wave number (k) was achieved using a calibration trace at 1.5 mm interferometer delay and numerical correction of the nonlinearly swept waveforms[27]. Image background subtraction and numeric compensation for second order dispersion[28] were performed. The complex SS-OCT data sets were upsampled by a factor of 4 and Fourier transformed. Axial motion correction was achieved on the obtained 2D and 3D SS-OCT data sets by cross correlating the consecutive horizontal tomograms. The mean and variance of the linear intensity, and logarithm of intensity were calculated for all voxels through acquired depth scans.

To perform motion contrast analysis and imaging, multiple B-scans were acquired over the same slice. Time separations were T_B=5 ms between B-scans for capturing the same position, respectively. Multiple linear intensity and phase measurements were recorded over the same transverse point separated in time. Two different intensity-based approaches were tested: speckle variance (SV)[20,21] and DLOGIV.

In the SV method, the linear amplitude mean (μ) and variance (σ^2) were calculated for the same transverse point acquired in successive B-scans (Fig. 2(b)). DLOGIV and DPV captured the differences between multiple logarithmic intensity ($LOG(I(z,T))$) and phase measurements ($\varphi(z,T)$) of the same transverse points (separated in time) and calculated the variance of these changes (Figs. 2(c) and 2(a)), respectively. To measure and remove timing-induced phase error[17] due to the random delay between the trigger signal and the subsequent A-to-D conversion (sample clock), a calibration signal was generated using a stationary mirror in the calibration arm (Fig. 1) as described by Vakoc[17]. The calibration signal was located at a depth of 2 mm in the OCT intensity image. The corrected phase differences between adjacent B-scans for the same transverse point at a given depth were calculated by subtracting the phase difference of the calibration signal, linearly scaled with the sample signal depth, from the measured phase differences (Fig. 2a)[17]. Phase unwrapping was performed on all measurements. A weighted mean algorithm[16] estimated and removed the bulk axial motion phase change error (Fig. 2a).

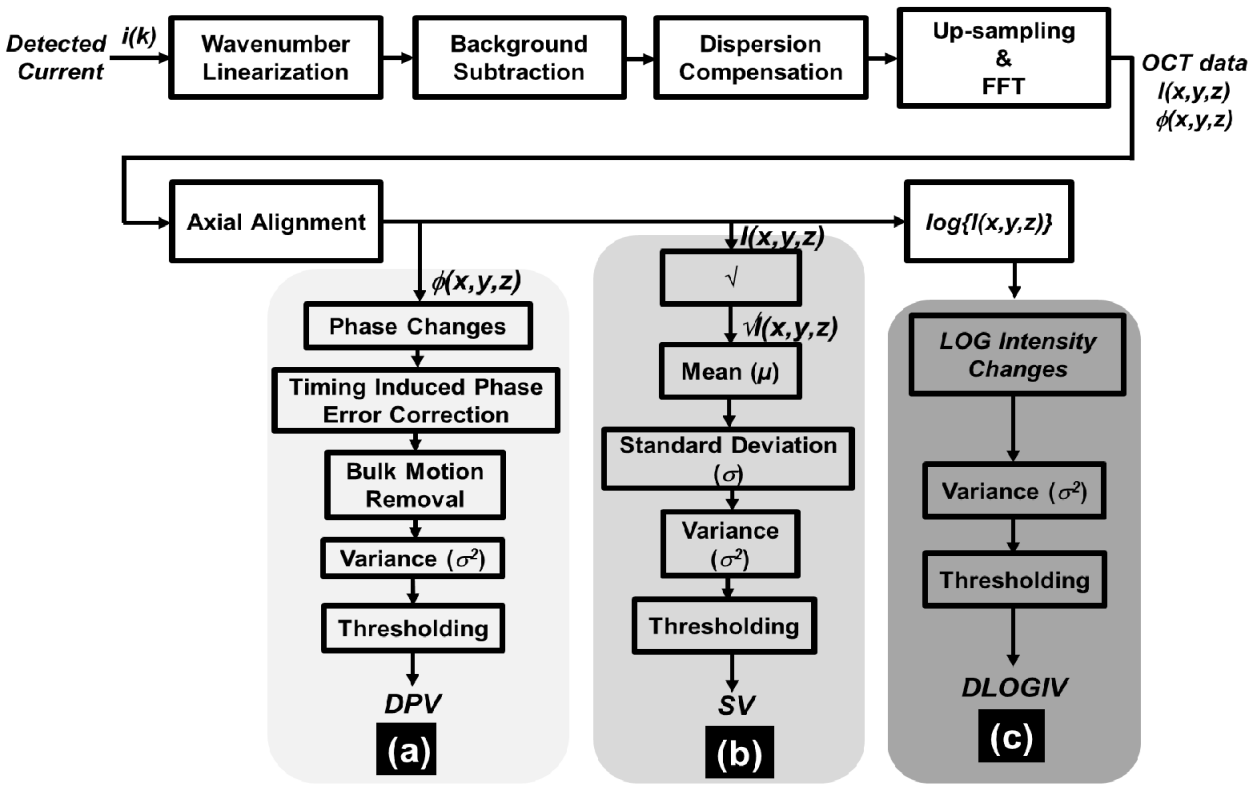

Fig. 2. Flowchart representing the data processing procedures for generating different motion contrasts of OCT: (a) DPV, (b) SV, and (c) DLOGIV.

The same described procedures were repeated for the adjacent transverse points in the same and neighboring B-scans to capture the retinal vasculature in 2D and 3D data sets. To remove SNR-limited intensity and phase change errors in2D and 3D data sets for vasculature visualization, an average intensity threshold (10 dB above the mean value of thenoise floor) was applied; all contrasts with average intensity values < mean ($\log_{10}(I_{noise})$) + 10 dB were set to zero in the corresponding images (Fig. 2). Additional processing was applied to the 3D contrast data sets using a moving average filter of ~5 μm in the axial direction and a median filter of ~8 μm radius in the transverse directions.

To create the retinal en face views, the inner/outer photoreceptor segments (IS/OS) and vitreoretinal interface were detected using a segmentation algorithm[10]. Three depth integrated motion contrast en face images were generated by integrating the SV, DLOGIV, and DPV between in the inner retina relative to IS/OS and vitreoretinal interface.

3. RESULTS

3.1 2D tomogram visualization of the retina using motion contrast imaging methods

To study different motion contrast methods, four B-scans were acquired across the foveal centralis (2 mm). The averaged intensity of four obtained B-scans is depicted in Fig. 3(a). While the SV (Fig. 3(b)) is able to capture the inner retina vessels (white arrow), it highlights the static regions of IS/OS and RPE (at the level of gray box) as motion. Motion in the inner choroid is barely detected in this tomogram. Figure 3(c) shows the enhanced motion contrast in 2D DLOGIV tomograms. White static areas (at the level of gray box) captured in 2D SV tomogram (Fig. 3(b)) are invisible in 2D DLOGIV tomogram (Fig. 3(c)). Regions of motion in the inner choroid (white band signified with blue boxes) and the small vessels in the inner retina (white arrows) are detectable in these 2D tomograms (Fig. 3(c)).

To compare the intensity-based contrasts with DPV contrast, 2D DPV tomograms are shown in Figs. 3(d)-3(e) before and after compensation, respectively. Figures 3(d) demonstrate DPV is unable to capture motion without use of compensation algorithms[16,17] and an extra hardware module[17]. In addition, the calibration mirror image limits imaging depth[17]. Thus, the simplicity and motion sensitivity of DLOGIV may make this contrast method more attractive than other proposed phase- and intensity-based methods[12-15, 18-21] for capturing motion and microvasculature.

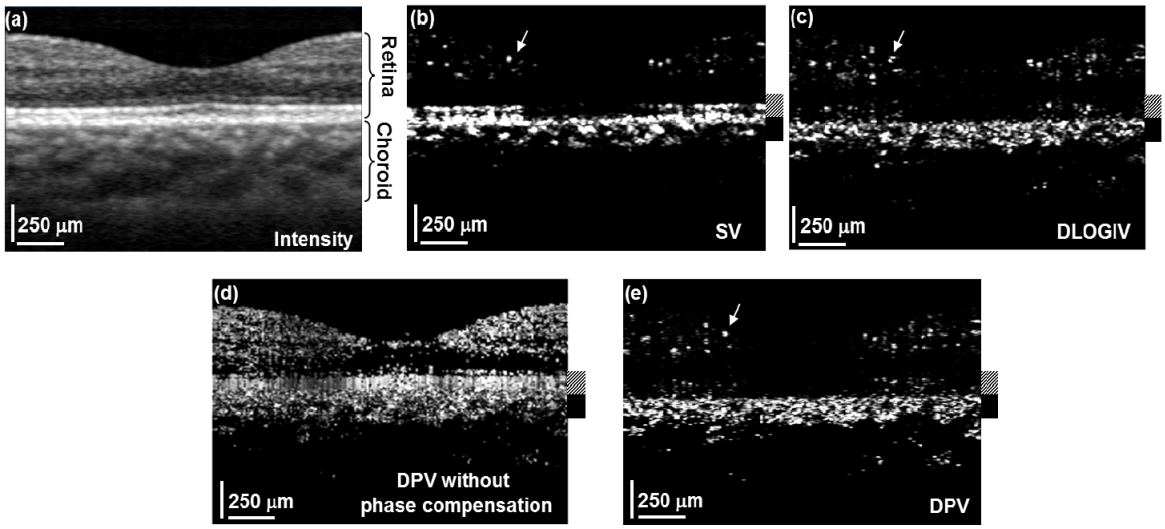

Fig. 3. Foveal (a) average intensity, (b) SV, (c) DLOGIV, (d) DPV before phase compensation, and (e) DPV after phase compensation 2D tomograms (2 mm). White regions correspond to regions with higher either motion or/and reflectivity. White arrows indicate the small vessel in Figs. 3(b)-3(e). Gray boxes signify IS/OS and RPE (static regions). Black boxes indicate regions of motion in the inner choroid.

3.2 En face view visualization of the retina using motion contrast imaging methods

Figures 4(a)-4(c) illustrate the intensity, DLOGIV, and DPV en face views generated by integrating their values between the region 30 μm posterior to the vitreoretinal interface and the region 130 μm anterior to IS/OS. Figure 4(a) shows that the meshwork of capillaries is barely visible in the intensity en face view. Motion contrast enhancement is depicted in Fig. 4(b) using DLOGIV method. Blood vessels in the ganglion cell layer and capillary meshwork of the inner plexiform layer are visualized in the DLOGIV en face view (Fig. 4(b)). FAZ is resolvable by considering the capillary network around it as shown in the DLOGIV images in Fig. 4(b). To compare retinal visualization using the proposed intensity-based motion contrast methods with the phase contrast method, the DPV en face image (Fig. 4(c)) is generated by summing DPVs over the same regions in the inner retina. Although DLOGIV and DPV en face images (Figs. 4(b)-4(c)) achieve the similar contrast for foveal vasculature visualization, DPV is a complicated method due to its need for the compensation algorithms[16,17] and an extra optical module[17].

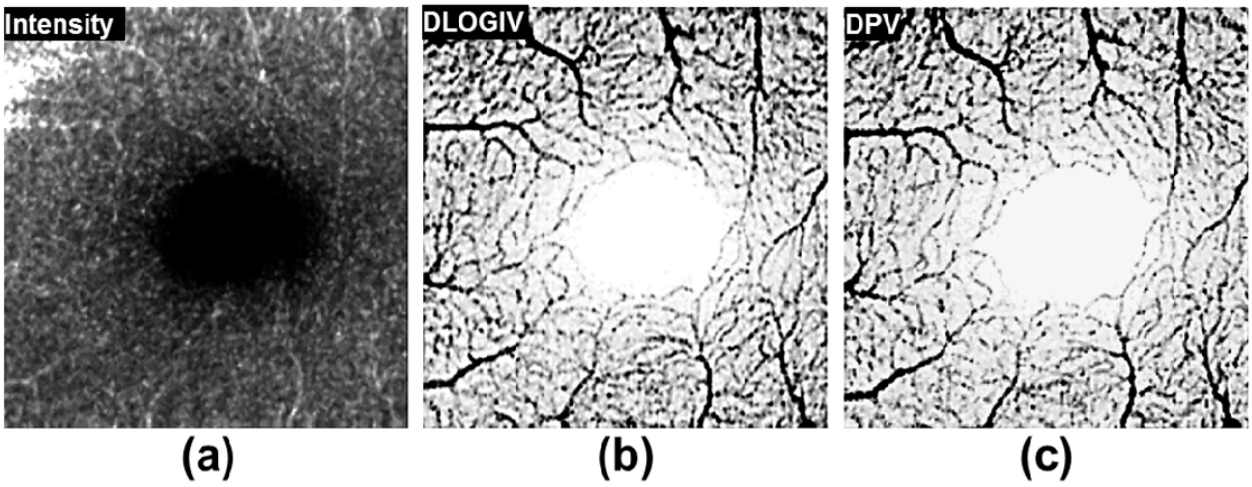

Fig. 4. Parafoveal depth-integrated en face views over 4 mm^2 FOV acquired in 4 seconds. (a) Averaged intensity, (b) DLOGIV, and (c) DPV en face images of the inner retina.

4. CONCLUSION

Our experimental result shows that the high sensitivity of speckle variance method to static regions degrades microvasculature visualization. Inability of the speckle variance method to distinguish the motion signals from structural signals would also limit their application in detecting leakage and abnormal vessels in patients with irregular retinal and choroidal vessels and structure. To improve upon these methods, we described a logarithmic intensity-based motion contrast method and demonstrated its superiority for *in vivo* human parafoveal microvasculature visualization. We could prove the feasibility of DLOGIV for non-invasive and dye-free visualization of the retinal microvasculature using a SS-OCT at 1060nm. Compared to DPV, DLOGIV does not rely on phase information. Therefore, it is less sensitive to the phase instability of the system and environment, and there is no need for phase compensation algorithms and additional optical modules. As such, DLOGIV may be advantageous to both DPV and invasive FA for imaging the retinal microvasculature and be a helpful diagnostic tool in the future.

5. ACKNOWLEDGMENTS

This work was supported in part by research from the California Institute for Regenerative Medicine (CIRM). The authors thank Carl Zeiss Meditec for providing the patient interface part of their Stratus OCT system.

REFERENCES

1. V. Patel, S. Rassam, R. Newsom, J. Wiek, and E. Kohner, "Retinal blood flow in diabetic retinopathy." BMJ. **305**(6855), 678–683 (1992)
2. E. Friedman, "A hemodynamic model of the pathogenesis of age-related macular degeneration," Am. J. Ophthalmol. **124**, 677–682 (1997).
3. J. Flammer, S. Orgul, V. P. Costa, N. Orzalesi, G. K. Krieglstein, L. M. Serra, J.-P. Renard, and E. Stefansson,"The impact of ocular blood flow in glaucoma," Prog. Retin. Eye Res. **21**, 359–393 (2002).
4. S. S. Hayreh, *Anterior Ischemic Optic Neuropathy*, (Springer-Verlag, 1975).
5. J. D. Gass, *Stereoscopic atlas of macular diseases*, 4th ed. (Mosby, 1997).
6. L. A. Yannuzzi, K. T. Rohrer, L. J. Tindel, R. S. Sobel, M. A. Costanza, W. Shields, and E. Zang, "Fluoresceinangiography complication survey," Ophthalmology **93**(5), 611–617 (1986).
7. M. Hope-Ross, L. Yannuzzi, E. Gragoudas, D. Guyer, J. Slakter, J. Sorenson, S. Krupsky, D. Orlock, and C. Puliafito, "Adverse reactions due to indocyanine green," Ophthalmology **101**, 529–533 (1994).
8. W. Drexler and J. G. Fujimoto, *Optical Coherence Tomography: Technology and Applications, Biological and Medical Physics, Biomedical Engineering*," (Springer, 2008).
9. M. Wojtkowski, V. Srinivasan, J. G. Fujimoto, T. Ko, J. S. Schuman, A. Kowalczyk, and J. S. Duker, "Three-dimensional retinal imaging with high-speed ultrahigh-resolution optical coherence tomography," *Ophthalmology* **112**(10), 1734–1746 (2005).
10. S. Makita, Y. Hong, M. Yamanari, T. Yatagai, and Y. Yasuno, "Optical coherence angiography," Opt. Express **14**(17), 7821–7840 (2006).
11. T. Schmoll, C. Kolbitsch, and R. A. Leitgeb, "Ultra-high-speed volumetric tomography of human retinal blood flow," Opt. Express **17**, 4166 (2009).
12. J. Fingler, R. J. Zawadzki, J. S. Werner, D. Schwartz, and S. E. Fraser, "Volumetric microvascular imaging of human retina using optical coherence tomography with a novel motion contrast technique," Opt. Express **17**(24), 22190–22200 (2009).
13. Shuichi Makita, Franck Jaillon, Masahiro Yamanari, Masahiro Miura, and Yoshiaki Yasuno, "Comprehensive in vivo micro-vascular imaging of the human eye by dual-beam-scan Doppler optical coherence angiography," Opt. Express **19**, 1271-1283 (2011).
14. A. Szkulmowska, M. Szkulmowski, D. Szlag, A. Kowalczyk, and M. Wojtkowski, "Three-dimensional quantitative imaging of retinal and choroidal blood flow velocity using joint Spectral and Time domain Optical Coherence Tomography," Opt. Express **17**(13), 10584–10598 (2009).
15. B. J. Vakoc, R. M. Lanning, J. A. Tyrrell, T. P. Padera, L. A. Bartlett, T. Stylianopoulos, L. L. Munn, G. J. Tearney, D. Fukumura, R. K. Jain, and B. E. Bouma, "Three-dimensional microscopy of the tumor microenvironment *in vivo* using optical frequency domain imaging," Nat. Med. **15**(10), 1219–1223 (2009).

16. M. C. Pierce, B. H. Park, B. Cense, and J. F. de Boer, "Simultaneous intensity, birefringence, and flow measurements with high-speed fiber-based optical coherence tomography," Opt. Lett. **27**, 1534-1536 (2002).
17. B. Vakoc, S. H. Yun, J. F. de Boer, G. J. Tearney, and B. E. Bouma, "Phase-resolved optical frequency domain imaging," Opt. Express **13**, 5483-5493 (2005).
18. R. K. Wang, L. An, P. Francis, and D. J. Wilson, "Depth-resolved imaging of capillary networks in retina and choroid using ultrahigh sensitive optical microangiography," Opt. Lett. **35**, 1467-1469 (2010).
19. R. K. Wang and L. An, "Multifunctional imaging of human retina and choroid with 1050-nm spectral domain optical coherence tomography at 92-kHz line scan rate," J. Biomed. Opt. **16**(5), 050503 (2011).
20. A. Mariampillai, B. A. Standish, E. H. Moriyama, M. Khurana, N. R. Munce, M. K. K. Leung, J. Jiang, A. Cable, B. C. Wilson, I. A. Vitkin, and V. X. D. Yang, "Speckle variance detection of microvasculature using swept-source optical coherence tomography," Opt. Lett. **33**(13), 1530–1532 (2008).
21. A. Mariampillai, M. K. K. Leung, M. Jarvi, B. A. Standish, K. Lee, B. C. Wilson, A. Vitkin, and V. X. D. Yang, "Optimized speckle variance OCT imaging of microvasculature," Opt. Lett. **35**(8), 1257–1259 (2010).
22. J. W. Goodman, *Statistical Optics*, (Wiley, 1985).
23. J. M. Schmitt, S. H. Xiang, and K. M. Yung, "Speckle in optical coherence tomography," J. Biomed. Opt. **4**(1), 95 (1999).
24. M. Pircher, E. Goetzinger, R. Leitgeb, A. F. Fercher, and C. K. Hitzenberger, "Speckle reduction in optical coherence tomography by frequency compounding," J. Biomed. Opt. **8**, 565–569 (2003).
25. B. Karamata, K. Hassler, M. Laubscher, and T. Lasser, "Speckle statistics in optical coherence tomography," J. Opt. Soc. Am. A **22**(4), 593–596 (2005).
26. E. C. Lee, J. F. de Boer, M. Mujat, H. Lim, and S. H. Yun, "In vivo optical frequency domain imaging of human retina and choroids," Opt. Express **14**, 4403 (2006).
27. Y. Yasuno, V. D. Madjarova, S. Makita, M. Akiba, A. Morosawa, C. Chong, T. Sakai, K.-P. Chan, M. Itoh, and T. Yatagai, "Three-dimensional and high-speed swept-source optical coherence tomography for *in vivo* investigation of human anterior eye segments," Opt. Express **13**(26), 10652–10664 (2005).
28. B. Cense, N. Nassif, T. Chen, M. Pierce, S. H Yun, B. Park, B. Bouma, G. Tearney, and J. de Boer, "Ultrahigh-resolution high-speed retinal imaging using spectral-domain optical coherence tomography," Opt. Express **12**, 2435–2447 (2004).